iScience

CellPress
OPEN ACCESS

Article

A pain-causing and paralytic ant venom glycopeptide

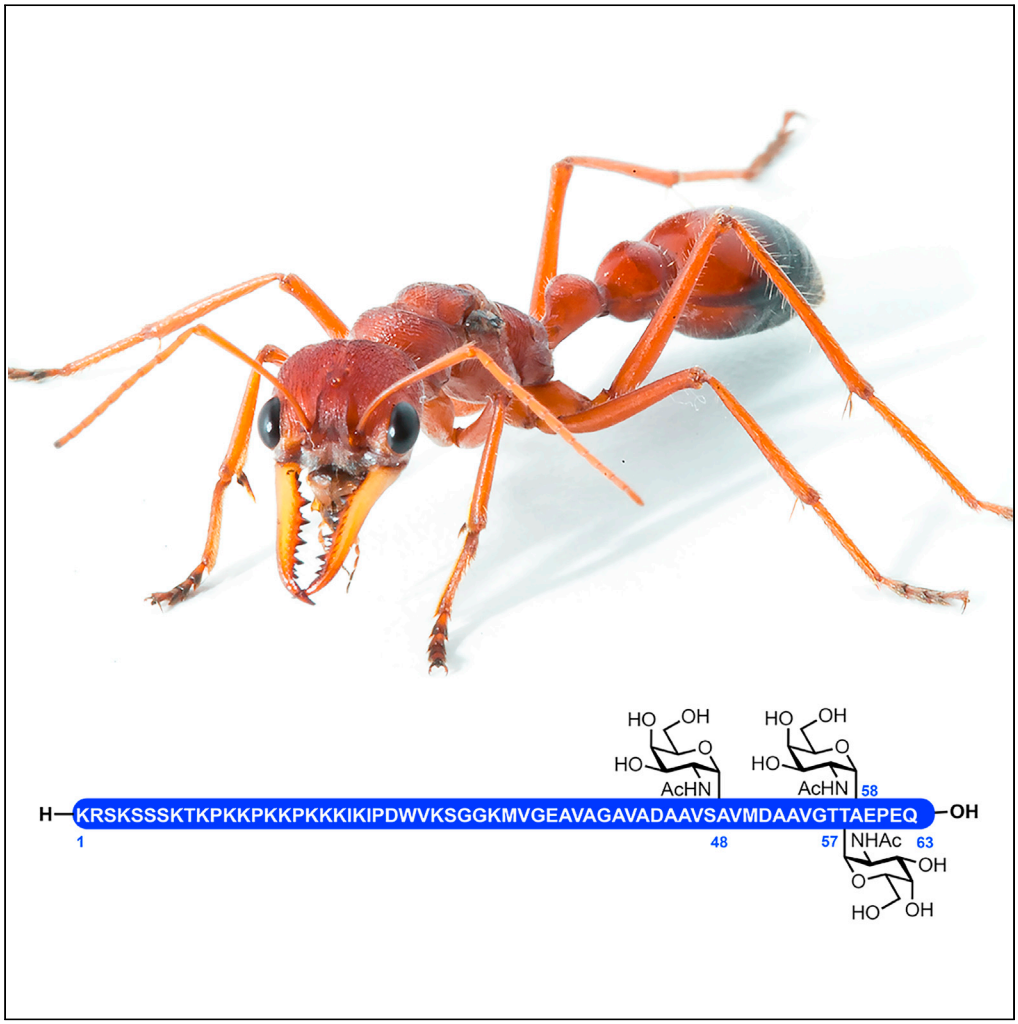

Samuel D. Robinson, Lucas Kambanis, Daniel Clayton, ..., Richard J. Payne, Glenn F. King, Eivind A.B. Undheim

sam.robinson@uq.edu.au (S.D.R.)
e.a.b.undheim@ibv.uio.no (E.A.B.U.)

Highlights

The 63-amino acid glycopeptide Mg7a is a major component of *Myrmecia gulosa* venom

Mg7a is insecticidal and causes pain behavior and inflammation in mice

Mg7a targets cell membranes causing a leak in ion conductance

Glycosylation is important for Mg7a solubility

Robinson et al., iScience *24*, 103175
October 22, 2021
https://doi.org/10.1016/j.isci.2021.103175

iScience

CellPress
OPEN ACCESS

Article

A pain-causing and paralytic ant venom glycopeptide

Samuel D. Robinson,[1,2,8,*] Lucas Kambanis,[3] Daniel Clayton,[3] Hannes Hinneburg,[4] Leo Corcilius,[3] Alexander Mueller,[2] Andrew A. Walker,[2] Angelo Keramidas,[2] Sameer S. Kulkarni,[3] Alun Jones,[2] Irina Vetter,[2] Morten Thaysen-Andersen,[4] Richard J. Payne,[3,5] Glenn F. King,[2,5] and Eivind A.B. Undheim[1,2,6,7,*]

SUMMARY

Ants (Hymenoptera: Formicidae) are familiar inhabitants of most terrestrial environments. Although we are aware of the ability of many species to sting, knowledge of ant venom chemistry remains limited. Herein, we describe the discovery and characterization of an *O*-linked glycopeptide (Mg7a) as a major component of the venom of the ant *Myrmecia gulosa*. Electron transfer dissociation and higher-energy collisional dissociation tandem mass spectrometry were used to localize three α-*N*-acetylgalactosaminyl residues (α-GalNAc) present on the 63-residue peptide. To allow for functional studies, we synthesized the full-length glycosylated peptide via solid-phase peptide synthesis, combined with diselenide–selenoester ligation-deselenization chemistry. We show that Mg7a is paralytic and lethal to insects, and triggers pain behavior and inflammation in mammals, which it achieves through a membrane-targeting mode of action. Deglycosylation of Mg7a renders it insoluble in aqueous solution, suggesting a key solubilizing role of the *O*-glycans.

INTRODUCTION

Numerous animals use venom to facilitate prey capture or to defend against predators, and there are over 100 independently evolved animal lineages (Schendel et al., 2019). Understanding the molecular basis of venom function can provide new insights into animal physiology and evolution (Zancolli and Casewell, 2020). Moreover, the potency and often favourable selectivity profiles of some venom peptides has led to their implementation as important research tools, and in some cases bioinsecticides (Smith et al., 2013), drug leads, and drugs (King, 2011; Robinson et al., 2017).

The majority of ant species are venomous and use their sting for prey capture and/or defense. Although ant species of the subfamily Formicinae spray an acid "venom" (Wray, 1670), there is accumulating evidence that the venoms of ants of 13 of the other 15 subfamilies are composed largely of peptides (Touchard et al., 2015) and that these peptides represent the major functional components of the venoms (Robinson et al., 2018; Touchard et al., 2020).

Although numerous ant venom peptides have now been reported (for reviews see (Aili et al., 2014; Touchard et al., 2016)) and their biomedical application as antimicrobials and antiparasitics is increasingly being pursued (For examples see (Cologna et al., 2013; Inagaki et al., 2004; Lima et al., 2016)), studies investigating the biological function and mode of action of ant venom peptides remain limited (Arseniev et al., 1994; Dekan et al., 2017; Duval et al., 1992; Heep et al., 2019; Inagaki et al., 2008; Nixon et al., 2020; Orivel et al., 2001; Piek et al., 1991; Pluzhnikov et al., 1999; Robinson et al., 2018).

Recently, we used transcriptomics and proteomics technologies to generate the first complete picture of the venom composition of an ant: that of the giant red bull ant *Myrmecia gulosa*, which delivers notoriously painful stings (Robinson et al., 2018). We revealed the major components of the venom which included, as described herein, an unusual 63-residue glycopeptide, Mg7a. In addition to the detailed characterization of the primary structure of Mg7a, we report its total chemical synthesis via diselenide–selenoester ligation-deselenization chemistry, characterize its biological function and mode of action, and demonstrate the critical role played by glycosylation in maintaining the aqueous solubility of the peptide.

[1]Centre for Advanced Imaging, The University of Queensland, St Lucia, QLD 4072, Australia

[2]Institute for Molecular Bioscience, The University of Queensland, St Lucia, QLD 4072, Australia

[3]School of Chemistry, The University of Sydney, Camperdown, NSW 2006, Australia

[4]Department of Molecular Sciences, Macquarie University, Macquarie Park, NSW 2109, Australia

[5]ARC Centre of Excellence for Innovations in Peptide and Protein Science, St Lucia, Australia

[6]Centre for Biodiversity Dynamics, Department of Biology, Norwegian University of Science and Technology, 7491 Trondheim, Norway

[7]Centre for Ecological and Evolutionary Synthesis, Department of Biosciences, The University of Oslo, 0316 Oslo, Norway

[8]Lead contact

*Correspondence: sam.robinson@uq.edu.au (S.D.R.), e.a.b.undheim@ibv.uio.no (E.A.B.U.)

https://doi.org/10.1016/j.isci.2021.103175

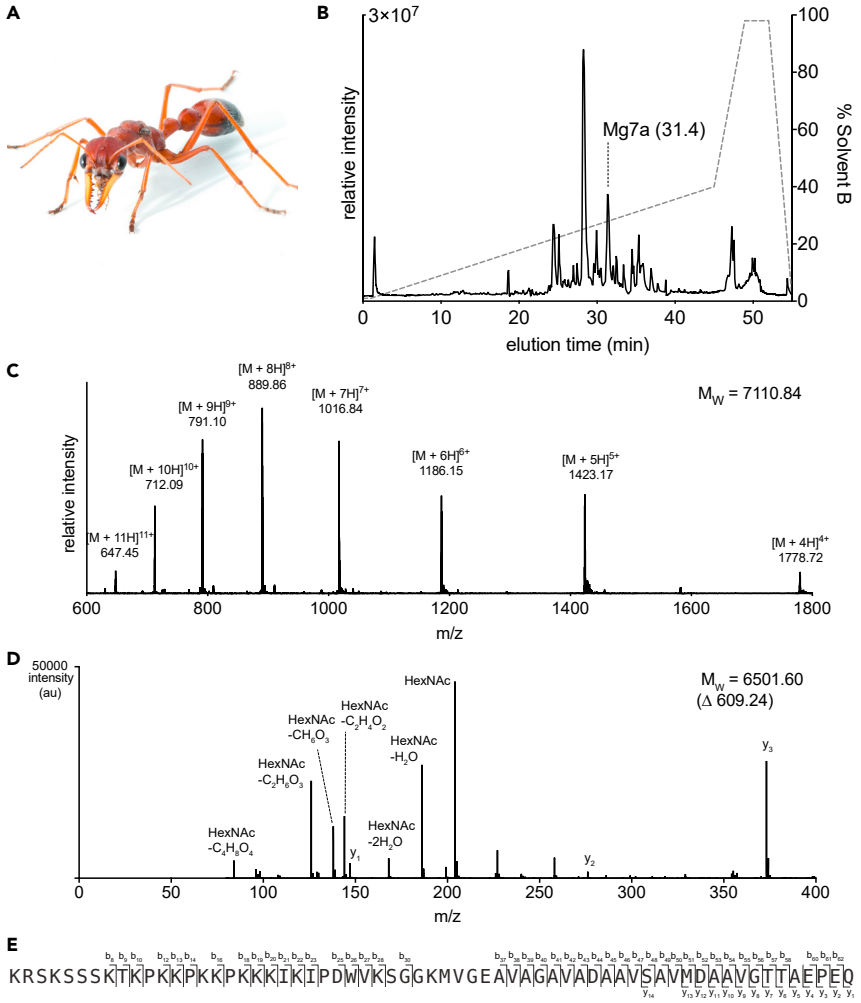

Figure 1. Mg7a, a 63-residue glycopeptide, is a major component of the venom of the giant red bull ant *Myrmecia gulosa*

(A) *M. gulosa*.

(B) LC-MS total ion chromatogram of *M. gulosa* venom. The labelled peak at 31.4 min corresponds to Mg7a.

(C) Precursor ions derived from a peak at 31.4 min. Charge series of +4 to +11 indicate a peptide with molecular mass of 7110.84 Da.

(D) CID-MS/MS (*m/z* range 0–400) spectrum of the $[M+8H]^{8+}$ precursor ion illustrating oxonium ions (for complete *m/z* range see S1).

(E) Ladder diagram of Mg7a illustrating b- and y-ions detected from MS/MS spectrum.

RESULTS AND DISCUSSION

Myrmecia gulosa venom contains a 63-residue glycopeptide

We first identified Mg7a as a major peak in the total ion chromatogram generated by liquid chromatography–mass spectrometry (LC-MS) of *M. gulosa* venom (Figure 1B). MS ions of charge series +4 to +11 indicated a product with a molecular mass of 7110.84 Da (Figure 1C). However, the corresponding fragment spectra from collision-induced dissociation (CID) MS/MS indicated a mass of 6501.60 Da (i.e. Δm = 609.24 Da) (Figures 1D and S1). The MS/MS spectrum showed excellent fragmentation of the peptide chain, but was dominated by ions at *m/z* 126.06, 138.06, 144.07, 186.07, and 204.8), which are diagnostic of *N*-acetylhexosamine (HexNAc) decomposition. This allowed us to deduce that Mg7a contains three HexNAc residues (609.24 Da) that were preferentially cleaved under CID. From the MS/MS data, we sequenced the peptide *de novo*, identifying an unambiguous stretch of 27 residues derived from the *C*-terminus and a partially ambiguous stretch of 22 residues from the *N*-terminus (Figure 1E). We used these sequences to

search a database derived from a venom apparatus transcriptome of *M. gulosa* (Robinson et al., 2018) and identified an exact match to a highly expressed transcript. This transcript encoded a prepropeptide composed of a signal sequence and propeptide region followed by a 63-residue mature peptide (Figures 1E and S2). The 63-residue mature peptide had a theoretical monoisotopic mass of 6501.60 Da, which matched the mass observed under CID (6501.60 Da; deconvolution of the $[M+5H]^{5+}$ ion observed in the MS/MS spectrum). Because addition of three HexNAc residues would yield a theoretical mass of 7110.84 Da, exactly matching the observed precursor ion (7110.84 Da; deconvolution of the $[M+8H]^{8+}$ ion), we concluded Mg7a included three HexNAc residues.

In addition to glycosylation, Mg7a has an unusual and striking primary structure (Figure 1E): its *N*-terminal half is extremely hydrophilic and cationic (net charge +14, with 14/32 Lys residues). In contrast, the *C*-terminal half is anionic (net charge −5) and dominated by small hydrophobic residues (19/31 are Ala, Val or Gly). When searched against the GenBank/SwissProt protein database using BLAST, no significant sequence similarity was detected, reflecting the distinctiveness of this peptide toxin.

The transcript encoding Mg7a was among the most highly expressed transcripts in the venom apparatus transcriptome, with an estimated expression level of 8,100 transcripts per million (TPM) (Figures S2C and S2D), comparable to other major venom peptides (Robinson et al., 2018). This suggested a key role for this peptide in the venom of *M. gulosa*. A further search of the venom-gland transcriptome revealed two closely related transcripts that we named Mg7b and Mg7c (Figure S2A). These transcripts also had high levels of expression (7,808 and 4,343 TPM, respectively). Analysis of LC-MS/MS data obtained from whole venom revealed the mature venom peptide Mg7b, for which MS and MS/MS data also indicated three HexNAc PTMs (data not shown). Although the mature peptides of Mg7a, Mg7b, and Mg7c are structurally unique, analysis of the precursor sequences i.e., the signal and pepropeptide domains indicates that the three peptides are derived from the aculeatoxin gene superfamily, which comprises a functionally diverse array of peptides from the venoms of the aculeate Hymenoptera (Robinson et al., 2018; Walker et al., 2018). Prepropeptide sequences of selected aculeatoxins are shown in Figure S2B for comparison with those of Mg7a, Mg7b, and Mg7c.

We used reversed-phase HPLC to purify Mg7a from *M. gulosa* venom (Figures S3A–S3C) and investigated the position and structure of the HexNAc residues using electron transfer dissociation (ETD)- and higher-energy collisional dissociation (HCD)-MS/MS of native and GluC-digested peptide. ETD-MS/MS, which retains labile peptide PTMs (including glycans) and thus can be used to localize them (Thaysen-Andersen et al., 2011), provided comprehensive coverage of the *N*-terminal 25 residues of the full-length peptide and demonstrated the absence of PTMs in this region (Figures S3D and S3E). After GluC digestion, several peptides were detected: the peptide WVKSGGKMVGE was identified in HCD-MS/MS and it also lacked glycosylation. The *C*-terminal end of the peptide was detected using ETD-MS/MS as two other GluC fragments (AVAGAVADAAVSAVMD and AAVGTTAEPEQ). MS and MS/MS data for these two peptides indicated the presence of one and two HexNAc residues, respectively (Figure S4), the positions of which were revealed as Ser48, Thr57 and Thr58. Ratiometric analysis of the oxonium ion profiles of these peptides generated under HCD-MS/MS indicated that the HexNAc were GalNAc residues (Figure S4) (Halim et al., 2014).

The unique and unusual primary structure of Mg7a (including glycosylation), combined with its high expression (and therefore likely functional importance in the venom of *M. gulosa*) motivated us to perform an in-depth investigation of its biological function and mode of action.

Synthesis of Mg7a by diselenide–selenoester ligation-deselenization chemistry

Having established the type and position of glycosylation in Mg7a, we embarked on its chemical synthesis to unequivocally confirm the structure predicted by mass spectrometry and transcriptomics, and to provide sufficient material for bioassays. We first attempted synthesis of the entire 63-residue peptide *via* Fmoc-based SPPS, however significant truncation of the sequence during iterative amino acid additions meant that the glycopeptide could not be generated in homogeneous form. We therefore turned to diselenide-selenoester ligation (DSL), coupled with deselenization chemistry (Kulkarni et al., 2019; Mitchell et al., 2015) to access Mg7a **1** (Figure 2A). Specifically, the sequence was disconnected between Gly40 and Ala41 which led to two requisite fragments: Mg7a(1–40) **2** functionalized as a *C*-terminal phenyl selenoester, and the diselenide dimer of Mg7a(41-63) **3** bearing an *N*-terminal selenocystine (the oxidized form of selenocysteine/Sec) and *O*-α-GalNAc residues at Ser48, Thr57, and Thr58. The two fragments were

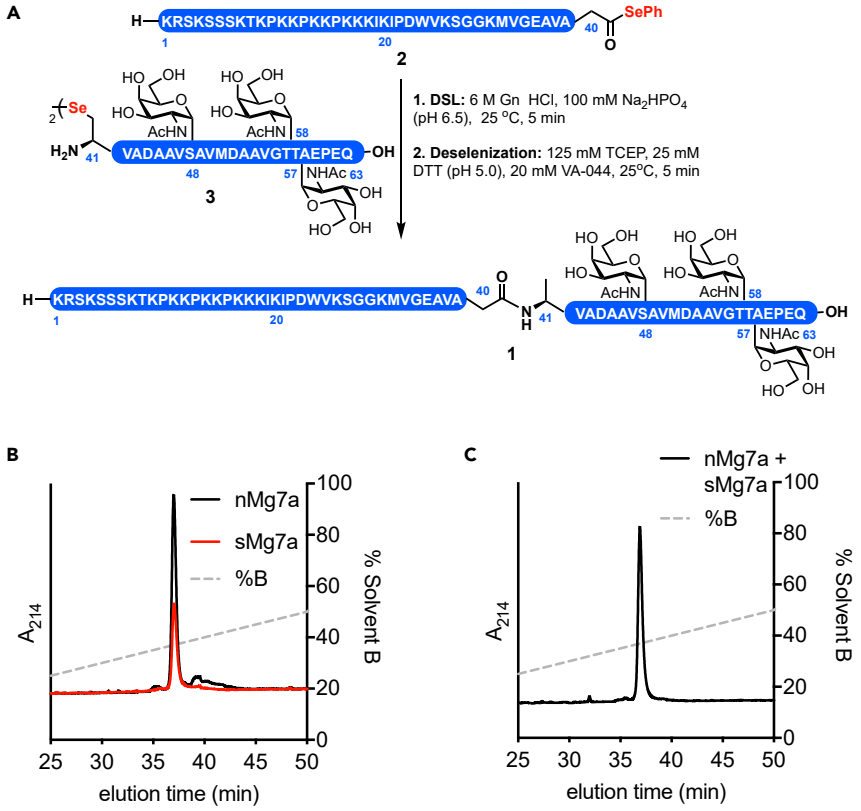

Figure 2. The glycopeptide Mg7a was synthesized by one-pot diselenide-selenoester ligation (DSL)-deselenization chemistry

(A) Synthesis scheme is shown in (A). Native and synthetic Mg7a had identical elution times on RP-HPLC.

(B) HPLC chromatograms (overlaid) of native Mg7a (~2 nmol) and synthetic Mg7a (~1 nmol; red).

(C) HPLC chromatogram of Mg7a (~2 nmol) co-injected with synthetic Mg7a (~1 nmol). Samples were analyzed on a Gemini NX-C18 column (250 × 4.6 mm; particle size, 3 μm; pore size, 110 Å; Phenomenex) using a gradient of 5–50% solvent B (90% MeCN and 0.05% TFA) over 45 min at a flow rate of 1 mL/min.

successfully synthesized *via* modified Fmoc-SPPS methods. The fragments were dissolved in a denaturing buffer comprising 6 M guanidine hydrochloride (Gn.HCl) and 100 mM sodium phosphate buffer at pH 6.5. Within 5 min the ligation had proceeded to completion as judged by LC-MS. Without purification, *tris*-carboxyethylphosphine (TCEP), dithiothreitol (DTT) and the water-soluble radical initiator, VA-044, were added to the reaction mixture to facilitate deselenization of the Sec residue at the ligation junction to alanine (Figure S5). Purification by reversed phase-HPLC, followed by lyophilization, afforded full-length, glycosylated Mg7a **1** in 38% yield (Figure S6). Importantly, the synthetic peptide co-eluted with native Mg7a on reversed phase-HPLC (Figures 2B and 2C) and displayed a matching CID-MS/MS profile (Figures S6E and S6F), providing strong evidence that the synthetic glycopeptide possesses identical primary structure, including GalNAc-α-Ser/Thr stereochemistry, to the native material isolated from the venom.

Mg7a is paralytic and lethal to insects and triggers pain behavior and inflammation in mammals

M. gulosa workers use their venom in both predation and defence. Adult workers are solitary hunters and generalists. Live prey items, which include insects such as flies (Diptera), Lepidoptera and other Hymenoptera (Wheeler, 1933), are first grasped with the well-developed mandibles and immediately incapacitated with the sting whereby they are returned to the colony to be fed to the carnivorous larvae. The ability of the sting to rapidly incapacitate prey is critical to the hunting strategy of *M. gulosa*. Consistent with a role in predation, intrathoracic injections of ≥5.6 nmol/g Mg7a into fruit flies (*Drosophila melanogaster*) induced rapid beating of the wings and uncoordinated flight attempts for several seconds, followed by loss of

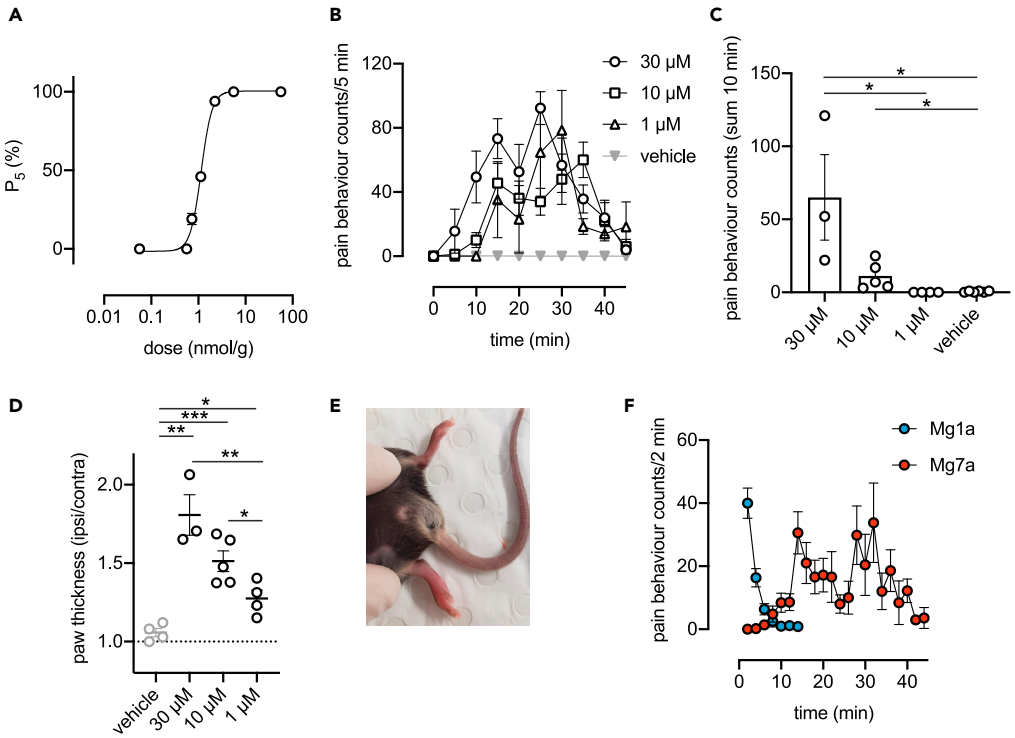

Figure 3. Mg7a paralyses fruit flies and induces pain behavior and inflammation in mice

(A) Intrathoracic injection of Mg7a is paralytic and lethal to fruit flies (EC_{50} 1.2 nmol/g). Each data point represents the percentage of flies immobilized (paralyzed or dead) at 5 min post-injection (P_5). Data are expressed as mean ± SEM (n = 3 experiments) and were fitted with a nonlinear regression with variable slope (four parameters).

(B) Intraplantar injection of Mg7a causes spontaneous dose-dependent nocifensive behavior in mice, lasting up to 45 min (n = 3–6 per group; data are expressed as mean ± SEM).

(C) The onset of pain behavior was dose-dependent. Differences between pain behavior counts summed over the first 10 min were analyzed using unpaired parametric t-tests.

(D) Mg7a causes dose-dependent paw swelling. Differences were analyzed using unpaired parametric t-tests.

(E) Representative swelling of injected right hindpaw (1 h post-injection) induced by 30 µM Mg7a.

(F) The time-course of pain behavior induced by Mg7a (1 µM) complements that of Mg1a (1 µM). *, $P < 0.05$; **, $P < 0.01$; ***, $P > 0.001$.

movement and death in 100% of flies, whereas lower doses induced reversible motor impairment with an ED_{50} of 1.2 nmol/g (Figure 3A).

Myrmecia sp. are notoriously aggressive and readily use their painful sting to deter potential predators. Mg7a also showed activity consistent with a defensive role, with intraplantar (i.pl.) injection of Mg7a (≥1 µM) in mice producing robust, dose-dependent pain behavior (i.e., licking, flinching or shaking of the paw; Figures 3B and 3C). The time course of pain behavior was characterized by a gradual increase, peaking at 25–35 min post-injection, and returning near to control levels by 45 min. In addition, injection of Mg7a produced a strong inflammatory response (redness and swelling) in the injected paw (Figures 3D and 3E). Notably, the time course of pain behavior complemented that of Mg1a, another *M. gulosa* venom peptide, which has immediate but short-lasting effects (Figure 3F) (Robinson et al., 2018). Together these data reveal that Mg7a likely plays a dual predatory and defensive role in the venom of *M. gulosa*.

Mode of action of Mg7a on mammalian cells

We next investigated the mode of action of Mg7a in the context of mammalian pain. In primary cell cultures from mouse dorsal root ganglia (DRG), which includes the neurons responsible for detecting painful stimuli, application of 1 µM Mg7a produced a rapid and sustained but variable-onset increase in intracellular calcium ($[Ca^{2+}]_i$) (Figures 4A and 4B) consistent with its ability to elicit pain behavior in mice. In primary DRG cultures, the increase in $[Ca^{2+}]_i$ occurred in both neuronal and non-neuronal cells, and although it did not occur in the absence of

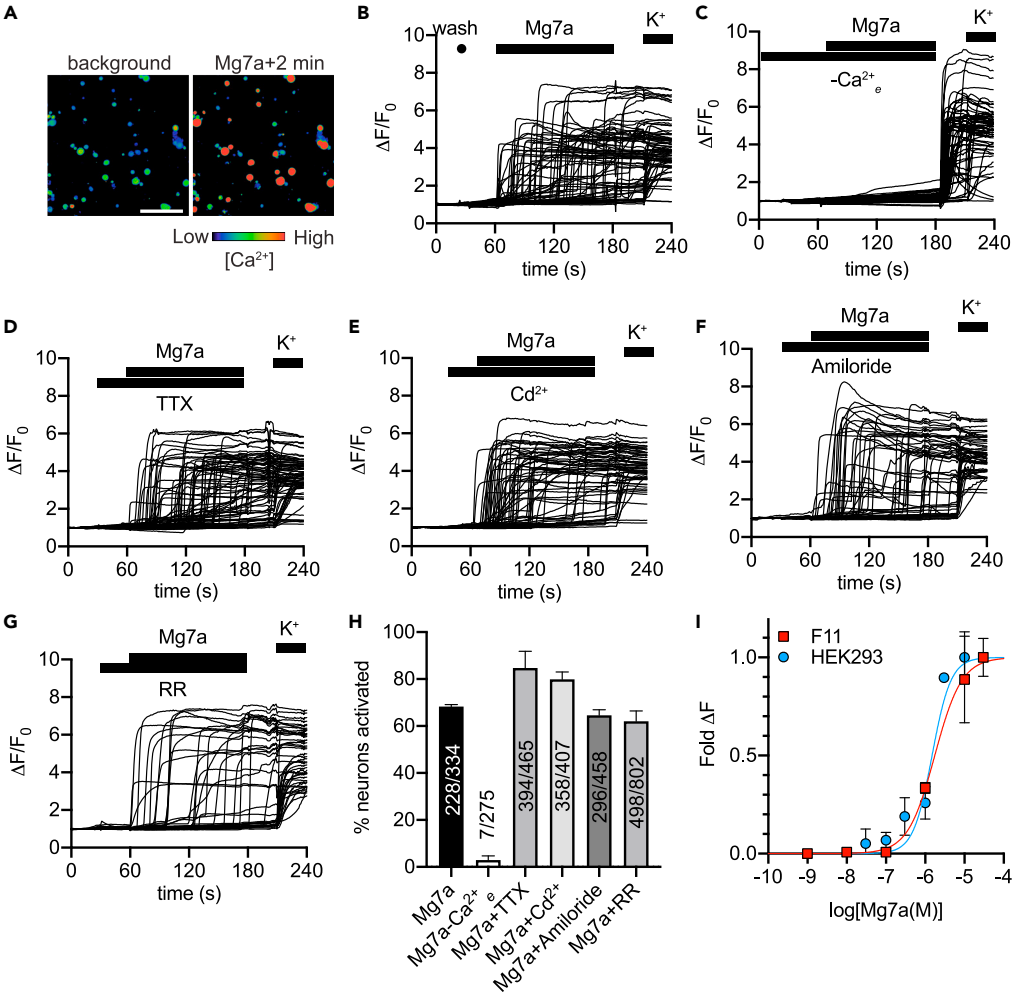

Figure 4. Mg7a activates mammalian sensory neurons

(A–B) Addition of Mg7a (1 μM) to mouse DRG neurons caused an increase in $[Ca^{2+}]_i$. The increase in $[Ca^{2+}]_i$ was rapid, but variable in onset, and observed in both neuronal and non-neuronal cells. Traces are from one representative experiment; scale bar = 100 μm.

(C–G) The increase in $[Ca^{2+}]_i$ was almost completely abrogated by the absence of extracellular Ca^{2+}, but unaltered by TTX (1 μM), Cd^{2+} (100 μM), amiloride (20 μM) or ruthenium red (RR; 20 μM).

(H) % of neurons activated, under each condition, by Mg7a in the 2-min window following addition. Data are expressed as mean ± SEM (n = 2). Total number of neurons from all experiments is indicated.

(I) Application of Mg7a to F11 and HEK293 cells caused a concentration-dependent increase in $[Ca^{2+}]_i$ with EC_{50} values of 1.75 and 1.49 μM, respectively. Data are expressed as mean ± SEM (n = 3).

extracellular Ca^{2+}, it was impervious to tetrodotoxin (TTX; 1 μM), a nonspecific blocker of voltage-gated sodium (Na_V) channels, cadmium (Cd^{2+}; 100 μM), a non-selective inhibitor of voltage-gated calcium (Ca_V) channels, amiloride (20 μM), a non-selective inhibitor of acid-sensing ion channels (ASICs), and ruthenium red (RR; 20 μM), a non-selective antagonist of transient receptor potential cation (TRP) channels and ryanodine receptors (Figures 4C–4H). Together, these data indicate that the activation of mammalian cells by Mg7a is because of influx of extracellular Ca^{2+} (intracellular stores do not contribute) and that voltage-gated sodium and calcium channels, ASICs, and TRP channels are not required, and points to a non-specific target for the peptide such as the cell membrane. The EC_{50} value for Mg7a, determined by fluorescence imaging in a mammalian sensory neuron cell line (F11 cells), was 1.75 μM (95% CI: 1.03 to 3.03 μM) (Figure 4I). Mg7a activated non-neuronal HEK293 cells (a human embryonic kidney cell line that does not express most of the ion channels found in DRG neurons and F11 cells) with comparable potency (1.49 μM; 95% CI: 1.00 to 2.27 μM) (Figure 4I), again consistent with a non-specific target for this peptide.

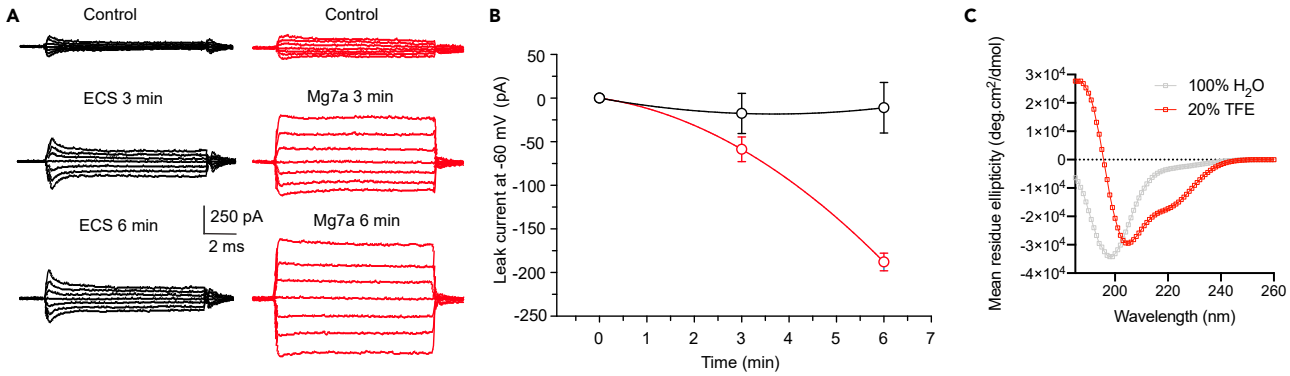

Figure 5. The mode of action of Mg7a is related to that of melittin

In HEK293 cells, Mg7a causes a time-dependent increase in leak current.

(A) Current traces +60 to −60 mV (20 mV steps) acquired before application and 3 and 6 min after application of ECS or Mg7a (20 nM).

(B) Change in leak current at −60 mV before and 3 and 6 min after addition of ECS (black) or Mg7a (20 nM; red). Data are expressed as mean ± SEM (n = 3–5 cells) and fitted to a second-order regression.

(C) Mg7a is unordered in water but adopts helical secondary structure in 25% TFE. Far-UV CD spectra (260–185 nm) of Mg7a (25 μM) in 100% H_2O and 20% TFE.

Other aculeatoxin peptides, including melittin from the venom of the European honeybee *Apis mellifera*, are known to exert their effects via the formation of ion-permeable "pores" in cell membranes (Okumura et al., 1981; Tosteson and Tosteson, 1981). Consistent with a similar mode of action, application of Mg7a to HEK293 cells caused a time-dependent increase in leak current: Leak current at −60 mV, 6 min after application of Mg7a (20 nM) was −188.0 ± 10.1 pA (n = 3 cells) compared with −11.1 ± 29.0 pA (n = 5 cells) for negative control (application of extracellular solution) (Figures 5A and 5B). Melittin and related peptides are structurally unordered in solution but adopt helical secondary structure when interacting with membranes or membrane-mimicking solvents such as trifluoroethanol (TFE) (Bazzo et al., 1988; Higashijima et al., 1983; Inagaki et al., 1989). Using circular dichroism (CD) spectroscopy, we investigated the secondary structure of Mg7a in water and in TFE. Far-UV (260–185 nm) CD data of Mg7a (25 μM) were consistent with a mostly unordered conformation in 100% H_2O, which shifted to partial helical conformation in TFE (20% v/v) (Figure 5C). These data indicate that, like its aculeatoxin counterparts, Mg7a has the capacity to adopt helical secondary structure when presented with a membrane-mimicking environment.

On the basis of these data, we propose a model whereby Mg7a interacts with mammalian cell membranes and produces a concentration and time-dependent leak in ion conductance, which in excitable cells such as sensory neurons leads to depolarization, action potential generation and nociception. Although this model explains the effects we observe when Mg7a is applied to mammalian cells, the possibility remains that a more specific mode of action mediated by one or more membrane proteins is responsible for the potent paralytic and lethal effects of the peptide on insects.

Glycosylation is critical to maintaining the aqueous solubility of Mg7a

We next sought to investigate the importance of the two halves of the peptide sequence and the role(s) of glycosylation on the activity of Mg7a. We used Fmoc-based SPPS to synthesize Mg7a(1-30) **4** and Mg7a(1-40) **5** *N*-terminal peptide fragments of Mg7a and the *C*-terminal glycopeptide fragment Mg7a(41-63) **6**, and tested the activity of each analogue in F11 cells. Each of the truncated peptides were inactive up to a concentration of 10 μM, (Figure 6D), indicating that the both "halves" of Mg7a are required for activity of the toxin.

Despite its lower structural complexity compared to the native tri-glycosylated Mg7a **1**, we were unable to prepare unglycosylated Mg7a. This was due to the lack of appreciable aqueous solubility of the *C*-terminal synthetic fragment under the ligation conditions. To overcome this challenge, we enzymatically deglycosylated the full-length synthetic Mg7a **1** using α-*N*-acetylgalactosaminidase (New England BioLabs) (Figures 3A and 3B). While the native tri-glycosylated Mg7a, and the truncated peptides Mg7a(1-30) **4**, Mg7a(1-40) **5** and Mg7a(41-63) **6** were soluble in water, reconstitution of the purified deglycosylated

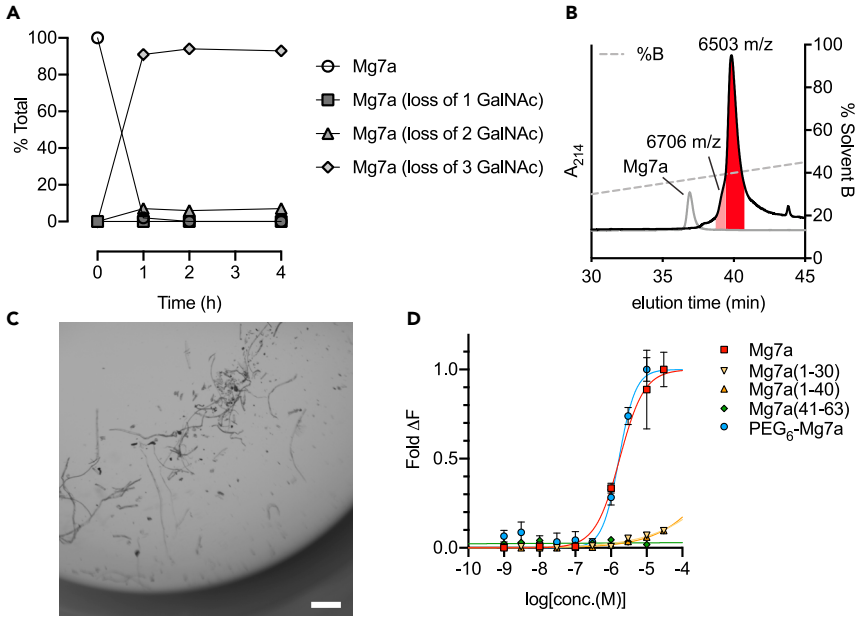

Figure 6. Glycosylation is critical to maintaining the aqueous solubility of Mg7a

(A) Enzymatic deglycosylation of Mg7a. Time-course of deglycosylation of Mg7a, as measured by relative ion count of glycoforms at 1, 2 and 4 h of treatment with α-*N*-acetylgalactosaminidase. At 1 h, only 2% of detected peptide was still fully glycosylated, while 91% was fully deglycosylated and 7% was partially deglycosylated (i.e., Mg7a with the loss of 2 GalNAc moieties). At 2 h, no fully glycosylated peptide was detected, and 94% was fully deglycosylated.

(B) Purification of deglyco-Mg7a by HPLC on a Gemini NX-C18 column (250 × 4.6 mm; particle size, 3 μm; pore size, 110 Å; Phenomenex) using a gradient of 5 to 50% solvent B (90% MeCN and 0.05% TFA) over 45 min at a flow rate of 1 mL/min. Mass of eluting peaks was confirmed by MALDI-MS (linear mode). Theoretical monoisotopic $[M+1H]^{1+}$ of Mg7a (loss of 2 GalNAc) = m/z 6705; Mg7a (loss of 3 GalNAc) = m/z 6503. Trace from Mg7a (fully glycosylated), run under the same conditions, is shown for comparison.

(C) Fibrillar precipitate formed upon reconstitution of deglycosylated Mg7a in water at a concentration of ~100 μM. Image was acquired on a Nikon DS-Qi2 microscope; scale bar = 100 μm.

(D) Activity of Mg7a and analogs on F11 cells. Data are expressed as mean ± SEM (n = 3).

full-length peptide in water or physiological salt solution (PSS) resulted in rapid formation of a fibrillar precipitate (Figure 6C).

Together these data suggested that the *O*-GalNAc residues play a critical role in maintaining the aqueous solubility of the peptide. The *C*-terminal half of Mg7a is dominated by small hydrophobic residues. For many venom peptides, hydrophobic patches are critical for interaction with their molecular target. Because the *C*-terminal stretch of hydrophobic residues is essential to the function of Mg7a, the addition of hydrophilic groups to this part of peptide, such as that provided by the *O*-GalNAc residues, could represent an adaptation to maintain its aqueous solubility. To test if the glycans contributed directly to the activity of the peptide, we used diselenide–selenoester ligation-deselenization chemistry to synthesize an analog of full-length Mg7a (**7**) with each of the native glycans substituted with a hexaethyelene glycol side chain (PEG_6Me) (i.e. at S48,T57,T58-PEG, see Figure S6). This analog was equipotent with the native glycosylated peptide toxin on F11 cells (1.67 μM; 95% CI: 1.39 to 2.71 μM) (Figure 6D), suggesting that although the glycans are critical for solubility of the full-length peptide, they do not directly contribute to its activity.

Limitations of the study

Our *in vitro* studies suggested that the mode of action of Mg7a in the context of mammalian pain was via direct disruption of cell membranes, which in mammalian sensory neurons could initiate depolarization, and result in nociception. This mode of action is consistent with what has been proposed for other related hymenopteran venom peptides like melittin or Mg1a (another major component of the venom of *M. gulosa*) (Robinson et al., 2018). But our data raise some unanswered questions: If Mg7a shares the same membrane-targeting mode of action as Mg1a, then why does it produce such a different time course of spontaneous

pain behavior? Does this "membrane-targeting" model also explain the paralytic/lethal effects observed in insects? On the basis of our data, we cannot completely rule out that a more specific receptor may exist (in mammals and/or insects), but that we are unable to observe it in our *in vitro* assays due to it being masked by the membrane-disrupting effects of the peptide. These questions are relevant for other apparent membrane-targeting peptides of hymenopteran and other venoms.

STAR★METHODS

Detailed methods are provided in the online version of this paper and include the following:

- KEY RESOURCES TABLE
- RESOURCE AVAILABILITY
  - Lead contact
  - Materials availability
  - Data and code availability
- EXPERIMENTAL MODEL AND SUBJECT DETAILS
  - Animals
  - Primary cell cultures
  - Cell lines
- METHOD DETAILS
  - Mass spectrometry of venom
  - Venom apparatus transcriptome
  - Mass spectrometry analysis of glycopeptide
  - Peptide synthesis materials and general procedures
  - Synthesis of Mg7a *N*-terminal selenoester (1–40) 2
  - Synthesis of Mg7a glycosylated *C*-terminal diselenide dimer (41–63) 3
  - Synthesis of Mg7a 1 through one-pot DSL-deselenization
  - Synthesis of Mg7a(1-30) 4 and Mg7a(1-40) 5 fragments
  - Synthesis of Mg7a(41-63) glycopeptide fragment 6
  - Synthesis of PEGylated Mg7a (PEG_6-Mg7a) 7 through one-pot DSL-deselenization
  - Enzymatic deglycosylation of Mg7a
  - Insecticidal assay
  - Pain behaviour experiments
  - Calcium imaging
  - Electrophysiology
  - Circular dichroism spectroscopy
- QUANTIFICATION AND STATISTICAL ANALYSIS
  - Insecticidal assay
  - Calcium imaging
  - Electrophysiology

SUPPLEMENTAL INFORMATION

Supplemental information can be found online at https://doi.org/10.1016/j.isci.2021.103175.

ACKNOWLEDGMENTS

This work was funded by the Australian Research Council (DECRA Fellowship DE160101142 to E.A.B.U.; Discovery Projects DP160104025 to E.A.B.U. and G.F.K., and DP190103787 to G.F.K., S.D.R, I.V.), the Australian National Health & Medical Research Council (Principal Research Fellowship APP1136889 to G.F.K. and Investigator Grant APP1174941 to R. J. P.) and the Norwegian Research Council (FRIPRO-YRT Fellowship no. 287462 to E.A.B.U.). H.H. was supported by a DFG postdoctoral fellowship, #357156333. M.T-A. was supported by a Macquarie University Research Seeding Grant. A.M. was supported by an Australian Government Research Training Program Scholarship.

AUTHOR CONTRIBUTIONS

Conceptualization, S.D.R. G.F.K. and E.A.B.U.; Methodology, S.D.R., A.K., I.V., M.T., R.J.P, G.F.K. and E.A.B.U.; Investigation, S.D.R., L.K., D.C., H.H., L.C., A.M., A.A.W., A.K., S.S.K. and A.J.; Writing – Original

Draft, S.D.R.; Writing – Review & Editing, All authors; Funding Acquisition, S.D.R., I.V., G.F.K. and E.A.B.U.; Resources, I.V., M.T., R.J.P, G.F.K. and E.A.B.U.; Supervision, I.V., M.T., R.J.P, G.F.K. and E.A.B.U.

DECLARATION OF INTERESTS

The authors declare no competing interests.

Received: August 3, 2020
Revised: September 7, 2021
Accepted: September 22, 2021
Published: October 22, 2021

REFERENCES

Aili, S.R., Touchard, A., Escoubas, P., Padula, M.P., Orivel, J., Dejean, A., and Nicholson, G.M. (2014). Diversity of peptide toxins from stinging ant venoms. Toxicon *92*, 166–178.

Arseniev, A.S., Pluzhnikov, K.A., Nolde, D.E., Sobol, A.G., Torgov, M.Y., Sukhanov, S.V., and Grishin, E.V. (1994). Toxic principle of selva ant venom is a pore-forming protein transformer. FEBS Lett. *347*, 112–116.

Bazzo, R., Tappin, M.J., Pastore, A., Harvey, T.S., Carver, J.A., and Campbell, I.D. (1988). The structure of melittin: a ^{1}H-NMR study in methanol. Eur. J. Biochem. *173*, 139–146.

Chisholm, T.S., Kulkarni, S.S., Hossain, K.R., Cornelius, F., Clarke, R.J., and Payne, R.J. (2020). Peptide ligation at high dilution via reductive diselenide-selenoester ligation. J. Am. Chem. Soc. *142*, 1090–1100.

Cologna, C.T., Cardoso Jdos, S., Jourdan, E., Degueldre, M., Upert, G., Gilles, N., Uetanabaro, A.P., Costa Neto, E.M., Thonart, P., de Pauw, E., et al. (2013). Peptidomic comparison and characterization of the major components of the venom of the giant ant *Dinoponera quadriceps* collected in four different areas of Brazil. J. Proteomics *94*, 413–422.

Dekan, Z., Headey, S.J., Scanlon, M., Baldo, B.A., Lee, T.H., Aguilar, M.I., Deuis, J.R., Vetter, I., Elliott, A.G., Amado, M., et al. (2017). Delta-Myrtoxin-Mp1a is a helical heterodimer from the venom of the jack jumper ant that has antimicrobial, membrane-disrupting, and nociceptive activities. Angew. Chem. Int. Ed. *56*, 8495–8499.

Duval, A., Malécot, C.O., Pelhate, M., and Piek, T. (1992). Poneratoxin, a new toxin from an ant venom, reveals an interconversion between two gating modes of the Na channels in frog skeletal muscle fibres. Pflügers Archiv. *420*, 239–247.

Halim, A., Westerlind, U., Pett, C., Schorlemer, M., Rüetschi, U., Brinkmalm, G., Sihlbom, C., Lengqvist, J., Larson, G., and Nilsson, J. (2014). Assignment of saccharide identities through analysis of oxonium ion fragmentation profiles in LC–MS/MS of glycopeptides. J. Proteome Res. *13*, 6024–6032.

Heep, J., Klaus, A., Kessel, T., Seip, M., Vilcinskas, A., and Skaljac, M. (2019). Proteomic analysis of the venom from the ruby ant *Myrmica rubra* and the isolation of a novel insecticidal decapeptide. Insects *10*, 42.

Higashijima, T., Wakamatsu, K., Takemitsu, M., Fujino, M., Nakajima, T., and Miyazawa, T. (1983). Conformational change of mastoparan from wasp venom on binding with phospholipid membrane. FEBS Lett. *152*, 227–230.

Inagaki, F., Shimada, I., Kawaguchi, K., Hirano, M., Terasawa, I., Ikura, T., and Gō, N. (1989). Structure of melittin bound to perdeuterated dodecylphosphocholine micelles as studied by two-dimensional NMR and distance geometry calculations. Biochemistry *28*, 5985–5991.

Inagaki, H., Akagi, M., Imai, H.T., Taylor, R.W., and Kubo, T. (2004). Molecular cloning and biological characterization of novel antimicrobial peptides, pilosulin 3 and pilosulin 4, from a species of the Australian ant genus Myrmecia. Arch. Biochem. Biophys. *428*, 170–178.

Inagaki, H., Akagi, M., Imai, H.T., Taylor, R.W., Wiese, M.D., Davies, N.W., and Kubo, T. (2008). Pilosulin 5, a novel histamine-releasing peptide of the Australian ant, *Myrmecia pilosula* (Jack Jumper Ant). Arch. Biochem. Biophys. *477*, 411–416.

Kambanis, L., Chisholm, T.S., Kulkarni, S.S., and Payne, R.J. (2021). Rapid one-pot iterative diselenide–selenoester ligation using a novel coumarin-based photolabile protecting group. Chem. Sci. *12*, 10014–10021.

King, G.F. (2011). Venoms as a platform for human drugs: translating toxins into therapeutics. Expert Opin. Biol. Ther. *11*, 1469–1484.

Kulkarni, S.S., Watson, E.E., Premdjee, B., Conde-Frieboes, K.W., and Payne, R.J. (2019). Diselenide–selenoester ligation for chemical protein synthesis. Nat. Protoc. *14*, 2229–2257.

Lima, D.B., Sousa, P.L., Torres, A.F., Rodrigues, K.A., Mello, C.P., Menezes, R.R., Tessarolo, L.D., Quinet, Y.P., de Oliveira, M.R., and Martins, A.M. (2016). Antiparasitic effect of *Dinoponera quadriceps* giant ant venom. Toxicon *120*, 128–132.

Mitchell, N.J., Malins, L.R., Liu, X., Thompson, R.E., Chan, B., Radom, L., and Payne, R.J. (2015). Rapid additive-free selenocystine–selenoester peptide ligation. J. Am. Chem. Soc. *137*, 14011–14014.

Nixon, S.A., Dekan, Z., Robinson, S.D., Guo, S., Vetter, I., Kotze, A.C., Alewood, P.F., King, G.F., and Herzig, V. (2020). It takes two: dimerization is essential for the broad-spectrum predatory and defensive activities of the venom peptide Mp1a from the jack jumper ant Myrmecia pilosula. Biomedicines *8*, 185.

Okumura, K., Inui, K.-I., Hirai, Y., and Nakajima, T. (1981). The effect of mastoparan on ion movement in black lipid membrane. Biomed. Res. *2*, 450–452.

Orivel, J., Redeker, V., Le Caer, J.P., Krier, F., Revol-Junelles, A.M., Longeon, A., Chaffotte, A., Dejean, A., and Rossier, J. (2001). Ponericins, new antibacterial and insecticidal peptides from the venom of the ant *Pachycondyla goeldii*. J. Biol. Chem. *276*, 17823–17829.

Piek, T., Duval, A., Hue, B., Karst, H., Lapied, B., Mantel, P., Nakajima, T., Pelhate, M., and Schmidt, J.O. (1991). Poneratoxin, a novel peptide neurotoxin from the venom of the ant, *Paraponera clavata*. Comp. Biochem. Physiol. C Comp. Pharmacol. *99*, 487–495.

Pluzhnikov, K., Nosyreva, E., Shevchenko, L., Kokoz, Y., Schmalz, D., Hucho, F., and Grishin, E. (1999). Analysis of ectatomin action on cell membranes. Eur. J. Biochem. *262*, 501–506.

Premdjee, B., Andersen, A.S., Larance, M., Conde-Frieboes, K.W., and Payne, R.J. (2021). Chemical synthesis of phosphorylated insulin-like growth factor binding protein 2. J. Am. Chem. Soc. *143*, 5336–5342.

Robinson, S.D., Mueller, A., Clayton, D., Starobova, H., Hamilton, B.R., Payne, R.J., Vetter, I., King, G.F., and Undheim, E.A.B. (2018). A comprehensive portrait of the venom of the giant red bull ant, *Myrmecia gulosa*, reveals a hyperdiverse hymenopteran toxin gene family. Sci. Adv. *4*, eaau4640.

Robinson, S.D., Undheim, E.A.B., Ueberheide, B., and King, G.F. (2017). Venom peptides as therapeutics: advances, challenges and the future of venom-peptide discovery. Expert Rev. Proteomics *14*, 931–939.

Schendel, V., Rash, L.D., Jenner, R.A., and Undheim, E.A.B. (2019). The diversity of venom: the importance of behavior and venom system morphology in understanding its ecology and evolution. Toxins *11*, 185.

Smith, J.J., Herzig, V., King, G.F., and Alewood, P.F. (2013). The insecticidal potential of venom peptides. Cell Mol. Life Sci. *70*, 3665–3693.

Thaysen-Andersen, M., Wilkinson, B.L., Payne, R.J., and Packer, N.H. (2011). Site-specific characterisation of densely O-glycosylated

mucin-type peptides using electron transfer dissociation ESI-MS/MS. Electrophoresis *32*, 3536–3545.

Tosteson, M.T., and Tosteson, D.C. (1981). The sting. Melittin forms channels in lipid bilayers. Biophys. J. *36*, 109–116.

Touchard, A., Aili, S.R., Fox, E.G., Escoubas, P., Orivel, J., Nicholson, G.M., and Dejean, A. (2016). The biochemical toxin arsenal from ant venoms. Toxins (Basel) *8*, 30.

Touchard, A., Aili, S.R., Tene, N., Barasse, V., Klopp, C., Dejean, A., Kini, R.M., Mrinalini, C.L., Jouenne, T., et al. (2020). Venom peptide repertoire of the european myrmicine ant *Manica rubida*: identification of insecticidal toxins. J. Proteome Res. *19*, 1800–1811.

Touchard, A., Koh, J.M.S., Aili, S.R., Dejean, A., Nicholson, G.M., Orivel, J., and Escoubas, P. (2015). The complexity and structural diversity of ant venom peptidomes is revealed by mass spectrometry profiling. Rapid Commun. Mass Spectrom. *29*, 385–396.

Vetter, I., and Lewis, R.J. (2010). Characterization of endogenous calcium responses in neuronal cell lines. Biochem. Pharmacol. *79*, 908–920.

Walker, A.A., Robinson, S.D., Yeates, D.K., Jin, J., Baumann, K., Dobson, J., Fry, B.G., and King, G.F. (2018). Entomo-venomics: the evolution, biology and biochemistry of insect venoms. Toxicon *154*, 15–27.

Wheeler, W.M. (1933). Colony-founding Among Ants: With an Account of Some Primitive Australian Species (Harvard University Press).

Wray, J. (1670). A letter concerning some uncommon observations and experiments made with an acid juyce to be found in ants. Philos. Trans. R. Soc. Lond. *5*, 2063–2066.

Zancolli, G., and Casewell, N.R. (2020). Venom systems as models for studying the origin and regulation of evolutionary novelties. Mol. Biol. Evol. *37*, 2777–2790.

STAR★METHODS

KEY RESOURCES TABLE

REAGENT or RESOURCE	SOURCE	IDENTIFIER
Chemicals, peptides, and recombinant proteins		
α-N-acetylgalactosaminidase	New England BioLabs	P0734S
Tetrodotoxin (TTX)	ABCAM Australia	ab120055
Cadmium chloride	Sigma Aldrich	202908
Amiloride	Sigma Aldrich	A7410
Ruthenium red	Sigma Aldrich	R2751
Critical commercial assays		
Fluo-4 AM calcium indicator	ThermoFisher Scientific	F36206
Calcium 4 assay	Molecular Devices	R8141
Deposited data		
Raw MS data	This paper	MassIVE: MSV000085353
Experimental models: cell lines		
F11 cell line	ATCC	HB-11761
HEK293 cell line	ATCC	CRL-1573
Experimental models: organisms/strains		
D. melanogaster: Canton S strain	Bloomington Drosophila Stock Center	Canton S
Mouse: C57BL/6	Animal Resources Centre	C57BL/6JArc
Software and algorithms		
GraphPad Prism	GraphPad	https://www.graphpad.com/scientific-software/prism/

RESOURCE AVAILABILITY

Lead contact

Further information and requests for resources and reagents should be directed to and will be fulfilled by the Lead Contact, Samuel D. Robinson (sam.robinson@uq.edu.au).

Materials availability

This study did not generate new unique reagents.

Data and code availability

- Prepropeptide sequences of Mg7a, Mg7b and Mg7c have been deposited with UniProtKB with accession codes Uniprot: P0DSK3, Uniprot: P0DPX0, and Uniprot: P0DSK4, respectively.
- Raw MS data for the discovery and characterisation of Mg7a has been deposited in MassIVE. The submission has received the accession number MSV000085353 (doi:10.25345/C50D92) and the data can be downloaded by ftp, using ftp://massive.ucsd.edu/MSV000085353/. (Reviewer ftp ftp://MSV000085353@massive.ucsd.edu)
- Any additional information required to reanalyze the data reported in this paper is available from the lead contact upon request.

EXPERIMENTAL MODEL AND SUBJECT DETAILS

Animals

- Adult workers of *M. gulosa* were collected near Brisbane, Queensland, Australia.

- *D. melanogaster* (Canton S strain) were cultured in 25 × 95 mm polypropylene culture vials, kept at room temperature (~23°C) on a 12/12 h light/dark cycle. Females 4-6 days post-eclosion were used for insecticidal activity assays.
- Male adult (6 weeks old) C57BL/6J mice used for behavioural experiments, were purchased from the Animal Resources Centre (WA, Australia), housed in groups of up to 4 per cage and maintained on a 12/12 h light-dark cycle and fed standard rodent chow and water *ad libitum*.

Primary cell cultures

- DRG cells were isolated from 4–6 week old male C57BL/6 mice, purchased from the Animal Resources Centre (WA, Australia). DRGs were dissociated and cells plated in Dulbecco's Modified Eagle's Medium (DMEM; Gibco, MD, USA) containing 10% fetal bovine serum (FBS) (Assaymatrix, VIC, Australia) and penicillin/streptomycin (Gibco) on a 96-well poly-D-lysine-coated culture plate (Corning, ME, USA) and maintained overnight.

Cell lines

- F11 (mouse neuroblastoma × DRG neuron hybrid) were cultured as previously described (Vetter and Lewis, 2010). Cells were maintained on Ham's F12 media supplemented with 10% FBS, 100 μM hypoxanthine, 0.4 μM aminopterin, and 16 μM thymidine (Hybri-MaxTM, Sigma Aldrich). 384-well imaging plates (Corning, Lowell, MA, USA) were seeded 24 h prior to calcium imaging, resulting in ~90% confluence at the time of imaging.
- HEK293 cells were cultured as previously described (Vetter and Lewis, 2010). Cells were maintained on DMEM supplemented with 10% heat-inactivated FBS, 2 mM L-glutamine, pyridoxine and 110 mg/mL sodium pyruvate. 384-well imaging plates (Corning, Lowell, MA, USA) were seeded 24 h prior to calcium imaging, resulting in ~90% confluence at the time of imaging.

METHOD DETAILS

Mass spectrometry of venom

Venom was collected by inciting ants to sting a thin layer of parafilm and droplets of venom collected in a small volume (10 μL) of pure water, quantified by absorbance at 280 nm and stored at -20°C. Venom (20 μg) was separated on a Shimadzu (Japan) Nexera uHPLC with an Agilent Zorbax stable-bond C18 column (2.1 mm × 100 mm, 1.8 μm particle size, 300 Å pore size), using a flow rate of 180 μL/min and a gradient of 1–40% solvent B (90 % acetonitrile [MeCN], 0.1% formic acid [FA]) in 0.1% FA over 30 min and analyzed on an AB Sciex 5600 TripleTOF mass spectrometer. MS survey scans were acquired at 300–1800 *m/z* over 250 ms, and the 20 most intense ions with a charge of +2 to +5 and an intensity of at least 120 counts were selected for MS/MS. The unit mass precursor ion inclusion window mass ± 0.7 Da, and isotopes within ±2 Da were excluded from MS/MS, with scans acquired at 80–1400 *m/z* over 100 ms and optimized for high resolution.

Venom apparatus transcriptome

A transcriptome derived from the venom apparatus tissue of *M. gulosa* was prepared as described (Robinson et al., 2018). Prepropeptide sequences of Mg7a, Mg7b and Mg7c have been deposited with UniProtKB with accession codes P0DSK3, P0DPX0, and P0DSK4, respectively.

Mass spectrometry analysis of glycopeptide

M. gulosa venom (500 μg) was separated on a Gemini NX-C18 column (250 × 4.6 mm; particle size, 3 μm; pore size, 110 Å; Phenomenex) using a gradient of 15 to 45% solvent B (90% MeCN and 0.05% trifluoroacetic acid [TFA]) over 30 min at a flow rate of 1 mL/min. Fractions were collected on the basis of absorbance at 214 nm and MALDI-MS was used to identify the fraction containing Mg7a. This fraction was separated again on a Onyx monolithic C18 column (100 × 4.6 mm; pore size, 130 Å; Phenomenex) using a gradient of 20 to 40% solvent B (90% MeCN and 0.05% TFA) over 20 min at a flow rate of 1 mL/min. Fractions were collected on the basis of absorbance at 214 nm and MALDI-MS was used to identify the sub-fraction containing Mg7a. The purity of this sub-fraction was assessed by reanalysis of an aliquot on the Gemini NX-C18 column using a gradient of 5 to 50% solvent B over 45 min at a flow rate of 1 mL/min.

An aliquot of purified Mg7a was digested using endoproteinase GluC (Sigma-Aldrich, MO, USA), according to the manufacturer's instructions (enzyme:peptide ratio of 1:100 in 100 mM NH_4HCO_3, pH 7.8, 37°C for 2 h). Peptide samples were either measured via direct infusion or separated on a 1260 Infinity system (Agilent Technologies) coupled to a HCT Ultra PTM Discovery system 3D ion trap with ETD and resonance activation CID (Bruker Daltonics, Bremen, Germany) or an Orbitrap Elite (Thermo Fischer Scientific) with HCD. Both instruments were operated in enhanced scan mode (high resolution mode) and in positive ion polarity.

Samples were taken up in 20 µL 0.1% FA (v/v), further diluted (1:10 in 0.1% FA, 50% MeCN [v/v]) and injected with a flow rate of 2 µL/min for direct infusion experiments. MS was operated with a 4–5 L/min dry gas flow, 300°C and a capillary voltage of 4–4.5 kV. The mass range was set to 180–2000 *m/z*, smart target at 200,000, SPS at 922 *m/z* with a maximum accumulation time of 50 ms allowed. Precursors of interest (isolation width of 4 Da) were manually selected and fragmented either with CID or ETD-MS/MS.

For LC-MS/MS setup 1 (ion trap), 5 µL samples of 1:10 diluted samples (see above) were separated on a C18 analytical column (PROTECOL, 100 mm × 300 µm ID, 5 µm, 300 Å, SGE Analytical Science) using a 4 µL/min flow rate with water containing 0.1% FA (v/v) as solvent A and 99% MeCN containing 0.1% FA (v/v) as solvent B. A linear gradient of 4.5%–55% solvent B in 76 min was applied followed by column washing and reconditioning. The top three most abundant precursors within the MS full scan range 400–1900 *m/z* were selected for either ETD or CID fragmentation with an isolation width of 2–3 Da and settings for smart target, SPS with a maximum accumulation time as mentioned above. Product ion spectra were acquired between 100–3000 *m/z*.

For LC-MS/MS setup 2 (Orbitrap), MS1 spectra were acquired with an Orbitrap Elite mass spectrometer (Thermo Fisher Scientific) in positive-ion mode over the *m/z* range 500–2000, with the automatic gain control (AGC) set to 10^6, maximum injection time of 200 ms, one micro scan, and resolution set at 120,000 (full width at half-maximum at 200 *m/z*). Source voltage was set to 3 kV, and capillary temperature to 310°C. MS/MS HCD spectra of the top ten most abundant peaks were recorded over an *m/z* range of 110–2000 at a resolution setting of 30000 after selection of the precursor within a 2-Da window and using a normalized collision energy (NCE) of 35%. AGC was at 50000.

Peptide synthesis materials and general procedures

Peptide-grade dimethylformamide (DMF) was obtained from Labscan. Fmoc-amino acids, coupling reagents and resins for Fmoc-based solid-phase peptide synthesis (SPPS) were obtained from either Novabiochem or GL Biochem.

Resin loading was determined by treating the resin with piperidine/DMF (1:4 v/v, 3 mL, 2 × 5 min) before washing with DMF (5 × 3 mL), CH_2Cl_2 (5 × 3 mL) and DMF (5 × 3 mL). The combined deprotection solutions were then made up to 10 mL with fresh piperidine/DMF (1:4 v/v). The solution was diluted 50-100 fold with fresh piperidine/DMF (1:4 v/v) and the UV absorbance of the piperidine-fulvene adduct measured (λ = 301 nm, ε = 7800 $M^{-1}cm^{-1}$) to estimate the amount of amino acid loaded onto the resin.

Preparative and semi-preparative reversed-phase HPLC was performed using a Waters 600E Multisolvent Delivery System with a Rheodyne 7725i Injection valve (4 mL loading loop) and Waters 500 pump with a Waters 490E programmable wavelength detector operating at 214, 230, 254 or 280 nm. A mobile phase of 0.1% TFA in water (Solvent A) and 0.1% TFA in MeCN (Solvent B) was used, with the linear gradients, flow rates and columns as specified. After lyophilization, peptides were isolated as fluffy white solid trifluoroacetate salts with the yields determined by dry weight.

Analytical RP-HPLC was performed on a Waters Acquity UPLC system equipped with PDA eλ detector (λ = 210–400 nm), Sample Manager FAN and Quaternary Solvent Manager (H-class) module. Peptides were analyzed using a Waters Acquity UPLC BEH 1.7 µm 2.1 × 50 mm column (C18) at a flow rate of 0.6 mL/min running on a mobile phase composed of 0.1% TFA in H_2O (Solvent A) and 0.1% TFA in MeCN (Solvent B) using a linear gradient as indicated. Analysis of chromatograms was performed using Empower 3 Pro software (2010) and retention times (R_t min) of pure peptides and proteins are reported with the gradients specified. Separations on the UPLC-MS system were performed using a Waters Acquity UPLC BEH 1.7 µm 2.1 × 50 mm column (C8) at a flow rate of 0.6 mL/min. Separations were performed using

a mobile phase of 0.1% formic acid in water (Solvent A) and 0.1% formic acid in MeCN (Solvent B) and a linear gradient of 0-50% B over 8 min. Low-resolution mass spectra were recorded on a Shimadzu 2020 mass spectrometer (ESI) operating in positive ion mode. MALDI mass spectra were acquired for the final purified glycosylated Mg7a 1 using linear mode on a Bruker (MA, USA) Autoflex™ Speed MALDI-TOF using a matrix of saturated α-cyano-4-hydroxycinnamic acid in 3:7 MeCN:H_2O containing 0.1% TFA (TA30), Equal volumes of the sample in TA30 and the matrix were mixed and spotted to a ground steel MALDI plate then allowed to dry. Data were acquired with Protein 1 calibrants (Bruker) then analyzed using Flexanalysis (Bruker) software.

Synthesis of Mg7a *N*-terminal selenoester (1–40) 2

Pre-swelled CEM Cl-TCP(Cl) heat-stable resin (100 μmol) was treated with a solution containing Fmoc-Gly-OH (300 μmol), 1.0 M *i*Pr_2NEt, and 0.125 M KI in DMF (25 mL) on a CEM Liberty Blue microwave peptide synthesizer at elevated temperature [cycle; 80°C for 60 s, then 90°C for 540 s], using conditions specified by the manufacturer. The resin was then capped *via* treatment with 17:2:1 v/v/v CH_2Cl_2:MeOH:*i*Pr_2NEt (5 mL) for 40 min at room temperature. The resin was then washed again with CH_2Cl_2 (5 × 3 mL), DMF (5 × 3 mL) and CH_2Cl_2 (5 × 3 mL) prior to determination of the loading of the first amino acid.

The peptide was elongated using microwave-assisted SPPS on a 100 mmol scale using a CEM Liberty Blue automated microwave peptide synthesizer (USA, NC). Peptide coupling cycles employed a mixture of Fmoc-protected amino acid (400 μmol), Oxyma (400 μmol) and *N,N′*-diisopropylcarbodiimide (DIC) (400 μmol) in DMF (0.1 M final concentration for all components after mixing). The Oxyma stock solution (0.3 M) also contained 0.1 M *i*Pr_2NEt in order to provide slightly more basic conditions to minimize loss of peptide from the CEM Cl-TCP(Cl) resin linker at high temperature. For most cycles, a 4 min high temperature method was employed [2 min coupling cycle (90°C), 1 min deprotection cycle (90°C), and 1 min associated with washes and liquid handling]. Ac-Gly-OH capping steps were introduced using similar conditions, and Fmoc-deprotection was performed by treatment with 20% v/v piperidine in DMF. This high temperature coupling and deprotection method was used until the Fmoc-Asp(O*t*Bu)-OH residue was incorporated (see sequence below) and then Fmoc deprotection was performed at room temperature by 2 × 3 min treatments using 20% piperidine in DMF containing 0.1 M 1-hydroxybenzotriazole (HOBt) to suppress aspartimide formation. A 50°C coupling method [20 min coupling (50°C), 2 × 3 min deprotection (rt), and 4 min associated washes and liquid handling] was used for the remainder of the synthesis including coupling of the final Boc-Lys(Boc)-OH residue (residues that were double-coupled are underlined: K<u>R</u>SKSSSK<u>T</u>KPKKPKKPKK<u>K</u>I<u>K</u>IPDW<u>V</u>KSGGKM<u>V</u>GE<u>AV</u>AG).

The resin was washed with CH_2Cl_2 (5 × 3 mL) before treating with a solution of hexafluoroisopropanol (HFIP)/CH_2Cl_2 (3:7 v/v, 4 mL) and shaken for 40 min at room temperature. The resin was filtered and washed with CH_2Cl_2 (3 × 3 mL). The combined cleavage solutions and washes were concentrated under nitrogen flow and dried *in vacuo*, to afford the crude sidechain-protected peptide with free *C*-terminal carboxylic acid.

The dry residue was dissolved in anhydrous DMF (1 mL per 25 μmol of resin) and cooled to 0°C. Ph_2Se_2 (30 equiv.) was added to the solution followed by Bu_3P (30 equiv.). The reaction was allowed to proceed at 0°C for 3 h, after which time the solvent was removed overnight under a stream of N_2. The crude material was put on ice and treated with TFA:*i*Pr_3SiH:H_2O (90:5:5 v/v/v) to remove the side chain protecting groups. After 2.5 h at room temperature the cleavage cocktail was removed under a stream of N_2 and the residue suspended in diethyl ether and cooled to 0°C. The precipitate was collected via centrifugation then gently dried under reduced pressure. The solid was then dissolved in 0.1% v/v TFA in H_2O (with minimal addition of MeCN to aid dissolution), analyzed by UPLC-MS (ESI) and purified by RP-HPLC using a 10–40% B gradient over 40 min on a Waters Sunfire C18 column (5 μm, 19 × 150 mm), at 15 mL/min to yield Mg7a *N*-terminal selenoester **2** as a fluffy white solid after lyophilization (20.4 mg, 4.69 μmol, 9.4% overall yield from initial resin loading).

Synthesis of Mg7a glycosylated *C*-terminal diselenide dimer (41–63) 3

The first residue was loaded onto *p*-alkoxybenzyl alcohol resin [Wang resin] (100 μmol) using a 3-fold molar excess of Fmoc-Gln(Trt)-OH (300 μmol), *O*-(Benzotriazol-1-yl)-*N,N,N′,N′*-tetramethyluronium hexafluorophosphate (HBTU) (300 μmol) and a 4.5-molar excess of *i*Pr_2NEt (450 μmol) in DMF (1 mL). A catalytic amount of 4-(dimethylamino)pyridine (DMAP) (10 μmol, in 500 μl of DMF) was added over 5 min to the

combined slurry of activated amino acid and resin. The resin was agitated gently for 18 h on an orbital shaker then drained and washed (5 × 5 mL) with DMF. Unreacted alcohol groups were capped with a mixture of acetic anhydride and iPr$_2$NEt in DMF (5:10:85 v/v/v), after which the resin was washed with DMF and a loading determination performed.

The peptide was assembled using a combination of stepwise Fmoc-SPPS on a Protein Technologies Symphony peptide synthesizer and off-instrument manual couplings of specialty building blocks (Boc-Sec(PMB)-OH and per-*O*-acetylated Fmoc-Thr[α-GalNAc]-OH/Fmoc-Ser[α-GalNAc]-OH). The synthesis was initiated at 100 μmol scale and reduced by half at several synthesis points to minimize specialty building block consumption and provide on-resin back-up material.

Peptide coupling cycles for non-specialty amino acids employed a mixture of Fmoc-protected amino acid (4 equiv.), Oxyma (4 equiv.) and DIC (4 equiv.) in DMF (0.1 M final concentration for all components after mixing). Coupling steps were performed for 45 mins at 25°C. Capping steps were introduced after each coupling step unless otherwise specified and performed by treatment with a 0.3 M Ac$_2$O/0.3 M iPr$_2$NEt solution in DMF (3 min). Fmoc-deprotection steps were performed by treatment of the resin with a 20% v/v piperidine solution in DMF at room temperature (2 × 3 min). Following each coupling, capping or deprotection step, the resin was washed with DMF (4 × 30 s). The underlined residues were double coupled: U<u>VADAAV</u>**S**(α-GalNAc)/<u>AVMDAAVG</u>**T**(α-GalNAc)**T**(α-GalNAc)AEPEQ-OH.

The resin was split to 50 μmol scale before installing the first Thr(α-GalNAc) residue, then split to 25 μmol scale before installing the Ser(α-GalNAc) residue. These residues were introduced *via* per-*O*-acetylated Fmoc-Thr[α-GalNAc]-OH/Fmoc-Ser[α-GalNAc]-OH building blocks as follows: A freshly-prepared solution of the Fmoc-glycosylamino acid (1.4 equiv.), *sym*-collidine (1.4 equiv.), 1-hydroxybenzotriazole (HOAt) (1.8 equiv.) and 2-(1*H*-7-azabenzotriazol-1-yl)-1,1,3,3-tetra-methyl uronium hexafluorophosphate (HATU) (1.4 equiv.) in dry DMF (0.05 M) was added to the resin and shaken at room temperature for 16 h. The resin was then washed with DMF (5 × 3 mL), CH_2Cl_2 (5 × 3 mL) and DMF (5 × 3 mL). The capping and deprotection steps were performed as detailed above.

For installation of the final Sec residue, a solution of Fmoc-Sec(PMB)-OH (2.0 equiv.), DIC (2.0 equiv.) and HOAt (2.0 equiv.) in DMF (0.1 M) was added to the resin and shaken at room temperature for 16 h (Premdjee et al., 2021). The resin was then washed with DMF (5 × 3 mL), CH_2Cl_2 (5 × 3 mL) and DMF (5 × 3 mL) and a capping step was performed as described above. Upon complete assembly of the peptide chain, the resin was washed with CH_2Cl_2 (5 × 30 s) and gently dried under vacuum.

The resin-bound peptide was treated with an ice-cold TFA:iPr$_3$SiH:water mixture (90:5:5 v/v/v, 5 mL) and allowed to shake at room temperature for 2 h. At this point, the resin was filtered and washed with fresh cleavage cocktail. The combined filtrates were concentrated under a stream of N_2 and the residue suspended in diethyl ether and cooled to 0°C. The precipitate was collected via centrifugation and then gently dried under reduced pressure.

The acetyl groups were removed from the GalNAc moieties by incubating the crude *C*-terminal peptide at 37°C in a solution containing 5 vol% hydrazine monohydrate and 25 vol% MeCN in H_2O (15 mg of crude peptide in 4 mL of solution). Removal of the acetyl groups was monitored by UPLC-MS and was complete after ~2 h. The solution was filtered and directly purified by preparative RP-HPLC with a 10–60% B gradient over 40 min, on a Waters Symmetry C4 (5 μm, 10 × 250 mm column; flow rate 4 mL/min) to yield the pure peptide as a fluffy white solid after lyophilisation.

The pure *p*-methoxybenzyl (PMB)-protected deacetylated selenopeptide was treated with a mixture of TFA:iPr$_3$SiH:thioanisole:H_2O (85:5:2:5 v/v/v/v) (6 mg lyophilised peptide in 6 mL of deprotection solution), containing 10 equiv. 2,2′-dithiobis(5-nitropyridine), and 150 equiv. Gn·HCl (Kulkarni et al., 2019). Conversion to the symmetrical diselenide was monitored by UPLC-MS and was complete after ~30 min. The TFA solution was then concentrated to a solid under a stream of nitrogen, and the peptide precipitated with a large volume of diethyl ether at 0°C for 60 min. The mixture was centrifuged and the resulting pellet dissolved in 0.1% v/v TFA in H_2O (with minimal addition of MeCN to aid dissolution), analyzed by UPLC-MS (ESI) and purified by RP-HPLC using a 5–55% B gradient over 40 min, using a Waters Symmetry C4 (5 μm,

10 × 250 mm) column at 4 mL/min, yielding the *C*-terminal diselenide dimer **3** (4.8 mg, 0.84 μmol, 6.7% overall yield).

Synthesis of Mg7a 1 through one-pot DSL-deselenization

A solution of Mg7a (41-63) diselenide dimer **3** (1.05 mg, 0.184 μmol, 0.5 equiv. [= 0.368 μmol, 1.0 equiv. of the monomeric selenopeptide]) in ligation buffer (6 M Gn·HCl, 100 mM Na_2HPO_4, adjusted to pH 6.3, 5 mM with respect to the monomeric selenopeptide) was added to Mg7a (1-40) selenoester **2** (2.15 mg, 0.479 μmol, 1.3 equiv. with respect to the monomeric selenopeptide). The resulting solution was carefully readjusted to pH 6.2-6.8 with 1 M KOH and the reaction incubated at 25°C for 5 min. Upon complete conversion to the corresponding ligation product (as assessed by UPLC-MS monitoring), an equal volume of a degassed solution of TCEP (500 mM) and dithiothreitol (50 mM) in buffer (6 M Gn·HCl, 100 mM Na_2HPO_4, pH 4-5) was added to the degassed ligation solution to give a final 250 mM concentration of TCEP, 25 mM concentration of dithiothreitol and 2.5 mM final concentration with respect to the peptide diselenide dimer starting material. VA-044 (1 mg) was then added and the solution reacted at 37°C. After complete deselenisation, as determined by UPLC-MS (∼5 min), 1 mL of ligation buffer was added to the reaction tube and the mixture was purified by RP-HPLC using a 5–55% B gradient over 40 min using a Waters Symmetry C4 (5 μm, 10 × 250 mm) column at 4 mL/min, yielding the full-length Mg7a glycopepide **1** as a fluffy white solid after lyophilisation (1.0 mg, 0.14 μmol, 38% yield).

For co-elution experiments, ∼2 nmol purified native Mg7a was analysed by HPLC on a Gemini NX-C18 column (250 × 4.6 mm; particle size, 3 μm; pore size, 110 Å; Phenomenex) using a gradient of 5–50% solvent B (90% MeCN and 0.05% TFA) over 45 min at a flow rate of 1 mL/min. This was then repeated with ∼1 nmol synthetic Mg7a and then a co-injection of the purified native Mg7a (∼2 nmol) and synthetic Mg7a (∼1 nmol) was performed.

For comparison of purified native and synthetic Mg7a CID MS/MS spectra, 2 μg of each were separated on a Shimadzu (Japan) Nexera uHPLC with an Agilent Zorbax stable-bond C18 column (2.1 mm × 100 mm, 1.8 μm particle size, 300 Å pore size), using a flow rate of 180 μL/min and a gradient of 1-50% solvent B (90% MeCN, 0.1% FA) in 0.1% FA over 14 min and analyzed on an AB Sciex 5600 TripleTOF mass spectrometer.

Synthesis of Mg7a(1-30) 4 and Mg7a(1-40) 5 fragments

Fmoc-Gly-OH was loaded onto Rink amide resin using *N,N′*-diisopropylcarbodiimide (DIC) and Oxyma in DMF (4-fold molar excess of each; 0.1 M final concentration) and the peptides were elongated (50 μmol scale) on a peptide synthesizer (Syro I automated synthesiser (Biotage)) using a 50°C coupling method [2 × 3 min deprotection, room temperature); 20 min coupling (50°C) and capping: 0.3 M Ac_2O/0.3 M iPr_2NEt solution in DMF (5 min, room temperature)]. The resin-bound peptides were treated with TFA:iPr_3SiH:water mixture (90:5:5 v/v/v, 5 mL) and allowed to shake at room temperature for 2 h. At this point, the resin was filtered and washed with fresh cleavage cocktail. The combined filtrates were concentrated under a stream of N_2 and the residue suspended in diethyl ether and cooled to 0°C. The precipitate was collected via centrifugation and then gently dried under reduced pressure. The crude peptides were then dissolved in 15% MeCN in H_2O (with 0.1% v/v TFA) and purified by RP-HPLC using a 0–60% B over 70 min gradient on an X-bridge C18 column (5 μm, 30 × 150 mm), at 38 mL/min to yield the desired peptides Mg7a(1-30) **4** and Mg7a(1-40) **5** as fluffy white solids after lyophilization [; Mg7a (1-30) **4**: 100 mg, 29 μmol, 58% overall yield from initial resin loading; Mg7a (1-40) **5:** 8 mg, 1.84 μmol, 4% overall yield from initial resin loading].

Synthesis of Mg7a(41-63) glycopeptide fragment 6

2-Chlorotrityl chloride resin [CTC resin] (1 g, 1.14 mmol/g, Mimotopes) was loaded by treating with a solution of Fmoc-Gln(Trt)-OH (550 μmol), and a 5-molar excess of iPr_2NEt (2.75 mmol) in CH_2Cl_2 (5 mL). The resin was agitated gently for 18 h on an orbital shaker then drained and washed with CH_2Cl_2 (5 × 5 mL). The resin was subsequently capped with a mixture of CH_2Cl_2/MeOH/iPr_2NEt (17:2:1 v/v/v, 4 mL) for 1 h before washing with DMF (5 × 3 mL), DCM (5 × 3 mL), and DMF (5 × 3 mL) and the amino acid loading determined to be 0.4 mmol/g. The synthesis of the target glycopeptide fragment was initiated on a 12.5 μmol scale. Peptide coupling cycles for standard amino acids involved Fmoc-protected amino acid (10 equiv.), Oxyma (11 equiv.) and DIC (10 equiv.) in DMF (0.25 M final concentration for all components after mixing). Coupling steps were performed for 1 h at 25°C. Coupling of Fmoc-Thr[α-GalNAc]-OH and Fmoc-Ser[α-GalNAc]-OH building blocks was performed as follows: A freshly-prepared solution of the

Fmoc-glycosylamino acid (1.4 equiv.), *sym*-collidine (1.4 equiv.), HOAt (1.8 equiv.) and HATU (1.4 equiv.) in dry DMF (0.05 M) was added to the resin and shaken at room temperature for 16 h. The resin was then washed with DMF (5 × 3 mL), CH_2Cl_2 (5 × 3 mL) and DMF (5 × 3 mL). A capping step was performed after each coupling step, which involved treatment of the resin with a 0.3 M Ac_2O/0.3 M iPr_2NEt solution in DMF (5 min). Fmoc-deprotection steps were performed by treatment of the resin with a 20% v/v piperidine solution in DMF at room temperature (2 × 5 min). Following each coupling, capping or deprotection step, the resin was washed with DMF (4 × 30 s). The underlined residues were double coupled: AVADAAV**S**(α-GalNAc)AVMDAAVG**T**(α-GalNAc)**T**(α-GalNAc)AEPEQ-OH.

NH_4I (100 mg) was next added to a solution of TFA:iPr_3SiH:H_2O:Me_2S (85:5:5:5, v/v/v/v, 2.0 mL), and the mixture was agitated for 5 min at room temperature. The resin-bound peptide synthesized above was treated with this solution, leaving behind the excess solid NH_4I, and the mixture was agitated at room temperature for 2 h. At this point, the resin was filtered and washed with fresh cleavage cocktail [TFA:iPr_3SiH:water (90:5:5, v/v/v)]. The combined filtrates were concentrated under a stream of N_2, during which a few drops of saturated sodium ascorbate solution were added, and the residue suspended in diethyl ether and cooled to 0°C. The precipitate was collected via centrifugation and then gently dried under reduced pressure. The acetyl groups were removed from the GalNAc units by incubating the crude glycopeptide in a solution containing 5 vol% hydrazine monohydrate and 25 vol% MeCN in H_2O (15 mg of crude peptide in 4 mL of solution) at 37°C. Deprotection of the acetyl groups was complete after ~2 h (as judged by UPLC-MS analysis of an aliquot of the reaction mixture). The solution was filtered and directly purified by preparative RP-HPLC with a 0–60% B gradient over 65 min, on a Waters Symmetry C4 (5 μm, 10 × 250 mm column; flow rate 4 mL/min) to afford the target Mg7a(41-63) glycopeptide **6** as a fluffy white solid after lyophilization (2.4 mg, 0.86 μmol, 6.9% overall yield).

Synthesis of PEGylated Mg7a (PEG_6-Mg7a) 7 through one-pot DSL-deselenization

A solution of PEGylated Mg7a(41–63) bearing an N-terminal DEAMC-protected Sec (1.9 mg, 0.56 μmol, 1.0 equiv.) in ligation buffer (6 M Gn·HCl, 100 mM Na_2HPO_4, adjusted to pH 6.3, 5 mM) was irradiated with 450 nm light for 15 min (PennOC photoreactor, 36 W) leading to complete DEAMC deprotection, as determined by UPLC-MS analysis (see Figure S6) (Kambanis et al., 2021). The solution was added to Mg7a (1-40) selenoester **2** (2.5 mg, 0.56 μmol, 1.0 equiv.) and the pH carefully readjusted to 5.8-6.3 with 1 M NaOH and the reaction incubated at 25°C for 10 min. Upon complete conversion to the corresponding ligation product (as assessed by UPLC-MS monitoring), extraction with diethylether (1 mL) was performed, followed by the addition of an equal volume of a degassed solution of TCEP (400 mM) and reduced glutathione (160 mM) in ligation buffer (6 M Gn·HCl, 100 mM Na_2HPO_4, pH 7.0) to the degassed ligation solution (final concentrations: 200 mM TCEP, 80 mM glutathione and 2.5 mM ligation product). The solution was then irradiated with 254 nm light for 7 min (PennOC photoreactor, 35 W). After complete photodeselenization (Chisholm et al., 2020) (as determined by UPLC-MS analysis) the reaction was diluted with 1 mL of ligation buffer before purification by RP-HPLC using a 0–60% B gradient over 65 min using a Waters Symmetry C4 (5 μm, 10 × 250 mm; flow rate 4 mL/min) at 40°C. Following lyophilization, PEG_6-Mg7a **7** was generated as a fluffy white solid (1.9 mg, 0.26 μmol, 46% yield).

Enzymatic deglycosylation of Mg7a

An aliquot of Mg7a was incubated with α-N-acetylgalactosaminidase (New England BioLabs, ME, USA) for 4 h at 37°C, according to the manufacturer's instructions. Deglycosylation was monitored by LC-MS: aliquots were taken at 1, 2 and 4 h, centrifuged to pellet the precipitate, diluted in 0.1% FA, and LC-MS data collected on an AB Sciex 5600 TripleTOF mass spectrometer (as described above under *Mass spectrometry of venom*). Ion counts were extracted based on theoretical $[M+8H]^{8+}$ ions of Mg7a (*m/z* 889.86), Mg7a – 1 GalNAc (*m/z* 864.48), Mg7a – 2 GalNAc (*m/z* 839.09) and Mg7a – 3 GalNAc (*m/z* 813.71). Peak maxima for each glycoform were normalized to total, to estimate the relative amounts of each glycoform present at each time point.

After the time course of deglycosylation was established, the experiment was repeated with an 80 μg aliquot of Mg7a. At 2 h, the sample was centrifuged to pellet precipitate, then the supernatant separated via HPLC on a Gemini NX-C18 column (250 × 4.6 mm; particle size, 3 μm; pore size, 110 Å; Phenomenex) using a gradient of 5–50% solvent B (90% MeCN and 0.05% TFA) over 45 min at a flow rate of 1 mL/min. The identity of eluting peaks was confirmed by MALDI-MS. Purified fully deglycosylated Mg7a was lyophilized and resolubilization was attempted in 100% H_2O and physiological salt solution (PSS; composition in

mM: 140 NaCl, 11.5 D-glucose, 5.9 KCl, 1.4 $MgCl_2$, 1.2 NaH_2PO_4, 5 $NaHCO_3$, 1.8 $CaCl_2$, 10 HEPES) (at a concentration of ~100 μM). The sample was analyzed visually for formation of precipitate and images acquired on a Nikon DS-Qi2 microscope.

Insecticidal assay

The insecticidal activity of Mg7a was assessed by intrathoracic injection into female *Drosophila melanogaster*. For each dose tested, three groups of eight female flies 4–6 days post-emergence were selected. Microinjection needles were prepared by pulling glass micropipettes (Drummond 3.5″ 3-000-203-GX) with a Sutter Instrument P-97 micropipette puller. The fine end was trimmed with scissors and the pipette filled with mineral oil using a syringe. The micropipette was then fitted on to a Kanetec Nanoliter 2000 autoinjector, and 2 μL of the solution to be injected was aspirated. Flies were immobilised by cooling for ~2 min and then placed on a petri dish filled with ice. Under a dissection microscope, each fly was impaled on the lateral thorax directly behind the wing, and 50.6 nL injected under automated control. Water was used as a negative control. Flies were then transferred, as a group of eight, to a 5 mL tube for observation. Paralysis was quantified by testing the ability of flies to climb off the bottom of the tube within 5 s after the tube was tapped gently on the bench five times to dislodge them. After the experiment, flies were frozen and weighed and their masses used to calculate the doses in nmol/g.

Pain behaviour experiments

Male adult (6 weeks old) C57BL/6J mice were used for behavioural experiments. Mg7a (20, 200 or 600 pmol) diluted in sterile saline containing 0.1% bovine serum albumin (BSA) was administered in a volume of 20 μL into the right hind paw by shallow (subdermal) intraplantar injection. Control animals were injected with vehicle (sterile saline containing 0.1% BSA). Spontaneous nocifensive events were counted from video recordings by a blinded observer. Paw thickness was measured by a blinded observer using electronic callipers at 1 h post injection. Experiments were approved by The University of Queensland animal ethics committee (UQ AEC).

Calcium imaging

Dissociated DRG cells, from 4–6 weeks old male C57BL/6 mice, were loaded with Fluo-4 AM calcium indicator, according to the manufacturer's instructions (ThermoFisher Scientific, MA, USA). After loading (1 h), the dye-containing solution was replaced with assay solution (1x Hanks' balanced salt solution, 20 mM HEPES). Images were acquired at 20x objective at 1 frame/s (excitation 485 nm, emission 521 nm). Fluorescence corresponding to $[Ca^{2+}]_i$ of 100–150 cells per experiment was monitored in parallel using a Nikon Ti-E Deconvolution inverted microscope, equipped with a Lumencor Spectra LED Lightsource. Baseline fluorescence was monitored for 30 s. At 30 s, assay solution was replaced with either assay solution, TTX (1 μM), Cd^{2+} (100 μM), Amiloride (20 μM) or RR (20 μM), then at 1 min with Mg7a (1 μM in assay solution ± TTX or $CdCl_2$) and monitored for 2 min before being replaced with assay solution and then KCl (30 mM; positive control). Experiments involving the use of mouse tissue were approved by UQ AEC.

F11 and HEK293 ells were incubated for 30 min with Calcium 4 assay component A according to the manufacturer's instructions (Molecular Devices, Sunnyvale, CA) in PSS at 37°C. Ca^{2+} responses were measured using a $FLIPR^{TETRA}$ fluorescent plate reader equipped with a CCD camera (Ex: 470–490 nm, Em: 515–575 nM) (Molecular Devices, Sunnyvale, CA). Signals were read every second for 10 s before, and 300 s after, the addition of peptide in PSS supplemented with 0.1% BSA. The resulting maximum-minimum florescence in the 300 s period after peptide was added was recorded as the response.

Electrophysiology

Voltage clamp recordings were performed at room temperature (22 ± 1°C) in standard whole-cell patch-clamp configuration, using HEK293-AD cells seeded onto poly-D-lysine-coated, 12 mm-diameter glass coverslips 1 d prior to experiments. The recordings were made using an EPC 10 USB Heka Patch Clamp Amplifier (HEKA, Elekronik), filtered (-3dB, 4-pole Bessel) at 2.9 kHz and sampled at 50 kHz. Patch electrodes were fabricated from borosilicate glass capillaries (G150F-3; Warner Instruments) and heat-polished to a final resistance of 2-4 MΩ when filled with intracellular solution. The intracellular solution was composed of (in mM): 145 CsCl, 2 $CaCl_2$, 2 $MgCl_2$, 10 HEPES, and 10 EGTA, adjusted to pH 7.4 with CsOH. The extracellular solution (ECS) comprised (in mM) 140 NaCl, 5 KCl, 2 $CaCl_2$, 1 $MgCl_2$, 10 HEPES and 10 D-glucose, adjusted to pH 7.4 with NaOH. Voltage protocol: From an initial clamped potential of

0 mV each recorded cell was subjected to a series of 10 ms voltage pulses that ranged from −60 to +60 mV in 20 mV increments. Recordings were made by perfusing each cell with ECS (t = 0 min) and at 3 min and 6 min of continuous perfusion of either ECS (control) or Mg7a (20 nM). Mg7a or ECS were delivered directly on to the recorded cell via plastic gravity-fed perfusion tubes.

Circular dichroism spectroscopy

Far UV CD spectra were recorded for Mg7a (25 μM) in 100% H_2O and in 20% TFE (*v/v*), using a Jasco J-810 CD spectropolarimeter (Easton, MD). Spectra were acquired from 260 to 185 nm, using a 1 mm path-length quartz cuvette, 1 nm step size, and averaging of 5 spectra.

QUANTIFICATION AND STATISTICAL ANALYSIS

Insecticidal assay

- Data are expressed as mean ± SEM and are representative of 3 experiments. Data were fitted with a nonlinear regression with variable slope (four parameters) in GraphPad Prism version 9.

Calcium imaging

- All data are mean ± SEM of 2-3 experiments. For EC_{50} calculations, a four-parameter Hill equation (Variable slope) was fitted using GraphPad Prism 9.

Electrophysiology

- Data are mean ± SEM of 3-5 experiments and fitted to a second-order regression.